**Development of window scheduler algorithm exploiting natural ventilation and thermal mass for building energy simulation and smart home controls**

Nari Yoon [1,*], Leslie Norford [2], Michael Wetter [3], Ali Malkawi [4]

1. Department of Architectural Engineering, University of Ulsan, Ulsan 44610, Republic of Korea
2. Massachusetts Institute of Technology, Department of Architecture, Cambridge, MA 02139, USA
3. Lawrence Berkeley National Laboratory, Energy Technologies Area, Building Technology and Urban Systems Department, Berkeley, CA 94720, USA
4. Harvard Center for Green Buildings and Cities, Cambridge, MA 02138, USA

*Corresponding author: Nari Yoon (nyoon@ulsan.ac.kr)

**Highlights:**

- A window scheduler algorithm using thermal network model is developed.
- The recommended window schedule is applied to a whole building simulation model.
- Different window schedules are suggested for different climates.
- The applications in EnergyPlus, Modelica, and smart buildings are discussed.

**Abstract**

Building energy simulations often rely on abstract assumptions when it comes to natural ventilation, such as 'windows always open [or closed]' or 'windows open when outdoor temperature is below a certain threshold.' However, simulations based on these assumptions fail to fully exploit the cooling potential of natural ventilation, as its effectiveness can be enhanced or diminished by various factors, including the presence of thermal mass. This issue also extends to smart home controls, where determining the window schedule becomes challenging without information about the building's response to outdoor conditions. To address these issues, this study has developed an analytical model for window operation schedules that leverages the passive cooling from natural ventilation. The analytical model was validated against a Modelica simulation. A case study utilizing the BESTEST model of ANSI/ASHRAE Standard 140 underwent validation with EnergyPlus simulations, showing strong concordance. The algorithm provides window schedule recommendations adapted to various airflow rates, thermal masses, and climate variations. The case study demonstrated that proper window scheduling could reduce indoor temperature by up to 8°C under the given simulation settings, thereby improving resilience and indicating potential energy savings. Furthermore, the paper explores the potential opportunities and challenges this approach presents, especially for building simulation and smart home applications.

Keywords: natural ventilation, thermal mass, smart window operation, optimization, thermal network model, window scheduler

## 1. Introduction

A window operation schedule is pivotal in building energy simulations, particularly when considering natural ventilation. However, identifying a schedule that effectively reduces cooling loads or moderates indoor air temperatures can be challenging. A recent survey by O'Brien et al. [1] on window operation schemes revealed that 42% of the 274 participants did not consider natural ventilation in their simulations. This omission was based on the assumption that windows were either always closed (19%) or inoperable (23%). Such an assumption can lead to significant overestimations of cooling loads, especially in designs that incorporate thermal mass as part of the building structure. Alternatively, keeping windows continuously open while a space is occupied is not the most desirable assumption, either. This is because there could be times when the outdoor temperature exceeds the preferred indoor comfort range, which may increase the cooling load. Another common assumption, accounting for 37% of the survey responses, was a window schedule based on indoor and outdoor temperatures. Under a steady-state assumption, a user might set a preferred outdoor temperature to operate windows. However, this approach might not always be effective. In many cases, room temperature is influenced not only by the outdoor temperature but also by factors like heat storage capacity of thermal mass, temperatures in adjacent zones, and heat gains from occupants, appliances, and solar radiation. As such, window operation schedules should be determined with a comprehensive understanding of factors that can impact the efficacy of natural ventilation.

Two aspects of window control for natural ventilation need to be considered. The first aspect is how occupants actually operate windows, while the second involves identifying the most appropriate schedules for window operation. Regarding the first aspect, various algorithms and probabilistic models have been studied to estimate occupant behavior for window operation. Lai et al. [2] studied the window-opening behavior of residents using the results obtained from measurements carried out for one year in various locations in China, and Pan et al. [3] analyzed nine months of monitored data for an office building to explore various factors that influence the window-opening behavior of occupants. Heracleous and Michael [4] monitored operation pattern in their experiment in a school, where they found that occupants tended to respond to outdoor temperature. Kim et al. [5] and Li et al. [6] suggested probability-based occupant behavior by logistic regression analysis, and Barthelmes et al. [7] applied the Bayesian network framework to model the window control behavior of occupants. In addition, many studies have examined machine learning approaches, including the XGBoost algorithm [8], deep learning [9], reinforcement learning [10], and instance-based learning paradigms [11] to better estimate the behavior of occupants.

Regarding the timing for window operations, several studies have investigated various control strategies. Wang et al. [12] and Weng et al. [13] utilized an outdoor air temperature threshold to control the window operations, while Landsman et al [14] and Roach et al. [15] used the indoor air

temperature set point in addition to the outdoor air temperature. Liu et al. [16] compared operative temperature to the outdoor temperature and comfort range guided by the American Society of Heating, Refrigerating and Air-Conditioning Engineers (ASHRAE) [17] to determine window actions. Furthermore, parametric studies with various operation schedules were conducted to identify window schedules [12], [18]. The challenge in determining the right window schedule is that an optimal indoor environment in the immediate future – i.e., the lowest indoor temperature in warm weather – cannot be guaranteed by opening or closing windows at a certain point based on indoor and outdoor temperatures alone, because of the sensitivity of the cooling effect to thermal mass, internal and solar heat gains, and airflow rates [19]. Testing every possible window operation schedule throughout a day is time-consuming, and finding a schedule for a certain day cannot be guaranteed to work for another day as weather changes. Therefore, we developed a physic-based analytical model to predict the consequences of opening and closing windows over the next control time step and formulate an algorithm to recommend windows operation at each control time step.

Analytical solutions for building energy performance serve various purposes, including parameterization, optimization, and performance control. Examples include building form optimization [20]–[22], building material optimization [23], [24], HVAC system controls [25], and combined and integrated modeling [26]–[28]. Furthermore, various analytical models have been developed to help explore the effects of natural ventilation on the thermal environment of buildings. Some researchers have suggested a single-zone analysis with different natural ventilation scenarios [29], multi-zone analysis under steady-state natural ventilation [30], study of flow patterns owing to buoyancy [31], and flow regime transition analysis [32], [33]. Many studies that considered thermal mass used the thermal-electrical analogy to investigate the thermal lag in buildings [23], [27], [34]–[36]. For example, heat transfer between multi-layered walls was calculated [27], [36], an external wall was optimized to minimize heating and cooling loads [23], a matrix exponential was derived to estimate thermal loads [34], and a single zone with mechanical ventilation was simulated [35].

The thermal-electrical analogy models have been demonstrated to effectively simulate the transient behavior of the building. However, many previous models predominantly focused on a building component or a single-zone building. While other analytical models for natural ventilation could analyze multi-zone buildings, their emphasis was primarily on the steady state. To achieve a broader applicability, a window control model should account for multiple zones or components, each with their distinct thermal heat capacities, while also capturing the transient behavior of buildings.

Therefore, this study developed a thermal-electrical analogy model for multi-zone/multi-mass buildings that considers thermal mass and natural ventilation over the upcoming control time step. A building with $n$ thermal resistances and $m$ thermal storages was represented by a concise $n$R–$m$C thermal network model. To verify the model, a test model was set up using Modelica, an equation-

based modeling language [37]. The model subsequently led to the development of a control algorithm that produced dynamic window operation schedules for passive cooling. We conducted case studies to explore the potential advantages of the schedule produced by the algorithm and demonstrate its practical applications. For these case studies, we utilized a BESTEST model [38] developed by following ANSI/ASHRAE Standard 140 using EnergyPlus [39]. We identified optimal natural ventilation schedules for four distinct climates and compared various operation modes for validation purposes.

## 2. Methodology

### 2.1. Quantitative analysis of multi-zone or multi-mass behavior

#### 2.1.1. Transformation of multi-zone problem into a single-zone problem

Prior to solving multiple zones or thermal masses, a single-zone model with one thermal mass and natural ventilation was reviewed. A model we investigate is a single room adjacent to another zone, namely Zone 1. The assumptions include that the room air is fully mixed; the room air temperature is close to the mass temperature; the internal convective and radiative heat gains from people, equipment, HVAC system, and sun are treated as a lumped heat gain; and the heat transfer through walls and air infiltration are treated as a lumped thermal resistance. These simplifications may not capture the full complexity of real-world scenarios, where heat sources are often distributed unevenly and the air may not be well-circulated. For example, heat from lighting fixtures may be concentrated near the ceilings, while solar heat through a window typically warms a localized area of the floor, resulting in a spatially variable temperature distribution. Some of these conditions can be addressed by treating each thermally significant element, such as a floor or a wall, as an individual thermal node in a more detailed model. This methodology is exemplified in the case study in Section 3. Nevertheless, for the foundational development of the model, the current set of assumptions is maintained for simplicity. With these assumptions in place, the room temperature $T_{\mathrm{rm}}$ at time $t$ can be written as

$$C_{\mathrm{rm}} \frac{dT_{\mathrm{rm}}}{dt} = \frac{\Delta T_1}{R_1} + Q_{\mathrm{rm}},$$  (1)

where  $C_{\mathrm{rm}}$: heat capacity of thermal mass of the room [J/K],
$T_{\mathrm{rm}}$: temperature of the test room [K],
$T_1$: Zone 1 temperature [K],
$\Delta T_1$: temperature difference between the room and Zone 1 [K/W],
$R_1$: thermal resistance between the room and Zone 1, accounting for conduction and infiltration [K/W],
$Q_{\mathrm{rm}}$: internal and solar heat gain rates of the room [W],

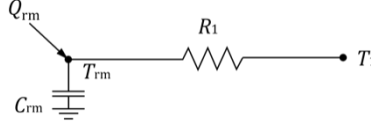and the thermal network of this case can be described as in Figure 1.



Figure 1. Circuit analogy of the 1R–1C model

When multiple wall properties exist between the room and Zone 1, $R_1$ can be the sum of thermal resistance from conduction through $k$ walls and convection owing to the air infiltration, which leads to

$$R_1 = \frac{1}{\sum_{j=1}^{k} U_j A_j + \rho\, C_p\, \dot{V}_1},$$
(2)

where $U_j$: overall heat transfer coefficient (U-value, W/m²-K) of the $j^{th}$ wall [W/m²-K],
$A_j$: area of the $j^{th}$ wall [m²],
$\rho$: density of air [kg/m³],
$c_p$: specific heat of air [J/kg-K], and
$\dot{V}_1$: airflow rates from Zone 1 to the room [m³/s].

Defining a time constant $\tau$ [s] as the product of the thermal resistance and heat capacity gives

$$\tau \equiv R_1\, C_{rm},$$
(3)

and multiplying both sides of Eq. (1) by $R_1$ leads to

$$\tau \frac{dT_{rm}}{dt} = T_1 - T_{rm} + R_1\, Q_{rm}.$$
(4)

Now, we consider a zone with $n$ adjacent zones. The thermal network is illustrated in Figure 2, and Eq. (1) can be updated to yield

$$C_{rm} \frac{dT_{rm}}{dt} = \frac{\Delta T_1}{R_1} + \frac{\Delta T_2}{R_2} + \cdots + \frac{\Delta T_n}{R_n} + Q_{rm},$$
(5)

where $\Delta T_n$: temperature difference between the room and Zone $n$ [K], and
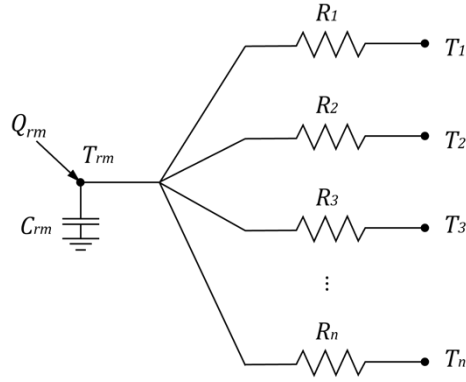$R_n$: thermal resistance between the room and Zone $n$ [K/W].

Figure 2. Circuit analogy of the $n$R–1C model

We define the new parameters

$$R^* \equiv \frac{1}{\Sigma_{j=1}^n \frac{1}{R_j}},$$ (6)

$$\tau^* \equiv R^* C_1,$$ (7)

$$T^* \equiv R^* \left( \Sigma_{j=1}^n \frac{T_j}{R_j} \right),$$ (8)

where $T_j$ is the indoor air temperature of the $j^{\text{th}}$ adjacent room, and $R_j$ is the thermal resistance between the room and its $j^{\text{th}}$ adjacent room. Multiplying both sides of Eq. (5) by Eq. (6) leads to

$$\tau^* \frac{dT_{\text{rm}}}{dt} = T^* - T_{\text{rm}} + R^* Q_{\text{rm}}.$$ (9)

Eq. (9) has the same form as Eq. (4). With a single thermal resistance, $R^* = R_1$, $\tau^* = \tau$, and $T^* = T_1$. Descriptively, $R^*$ and $T^*$ are the collective thermal resistance and collective air temperature of the neighboring zones, respectively, that transform a multi-zone problem into a single-zone problem, as illustrated in Figure 3.
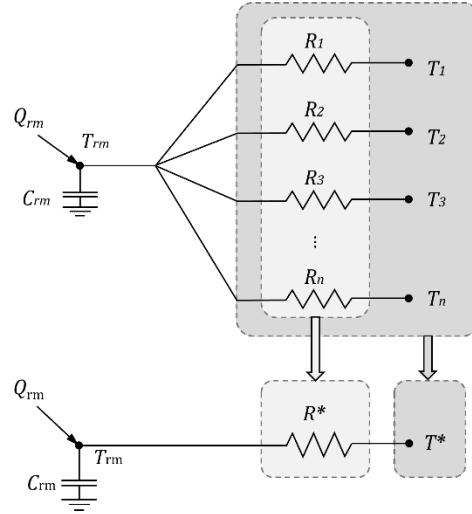
Figure 3. Transformation of a multi-zone solution into a single-zone solution

### 2.1.2. Prediction of room temperature in the upcoming time step

To predict the room temperature in the next time step, the following assumptions were made:

- The temperature of adjacent zones, ventilation rates, and internal and solar heat gains were constant during each time step; these inputs were then adjusted for the next discrete interval. Because the airflow rate $\dot{V}$ can vary by a time step, $R$ and $\tau$ also vary with time.
- The thermal resistance between air and the thermal mass of a zone is negligible such that the resultant temperature of the thermal mass and the zone's air are nearly equivalent. This assumption can be later relaxed with proper zoning methods, for example, treating each wall as an individual zone rather than a resistance.

With these assumptions and Eq. (9), the room temperature at the $(i+1)^{\text{th}}$ time step can be expressed as

$$T_{\text{rm},i+1} = T_{\text{rm},i}\, e^{-\frac{t}{\tau_i^*}} + \left(T_i^* + R_i^*\, q_{\text{rm},i}\right)\left(1 - e^{-\frac{t}{\tau_i^*}}\right), \tag{10}$$

where $n$ thermal resistances and neighboring zones are integrated into the collective parameters $R^*$ and $T^*$. The derivation of the formula is presented in Appendix A. The neighboring zones may or may not interact with each other. Some adjacent zones can be assumed to have fixed temperature profiles (e.g., outdoor and ground temperatures from the weather file, or the HVAC-controlled temperature), and other zones can be free-floating. Some neighboring zones may have thermal masses.

Finally, when thermal mass is present in $m$ neighboring zones, the above circuit analogy model becomes the $n$R–$m$C model. Each neighboring zone can also be expressed using Eq. (10), with its

8

parameters refined based on Eqs. (6)–(8). The $n$R–$m$C model is also adaptable to a single-zone model, particularly where $m$ distinct thermal masses are situated in various parts of the room. For example, a roof may possess a significantly different thermal heat capacity than a slab material. Furthermore, the roof might be exposed to a considerably different amount of solar radiation compared to the slab, which only receives radiation that is transmitted through the windows. In such situations, treating different masses as a single-integrated heat capacity could introduce inaccuracy. Instead, each material with its unique thermal mass can be represented as an individual zone within the $n$R–$m$C model.

## 2.2. Verification of nR–mC model

To ensure that the analytically derived model is free of error and the Python code for the model has been correctly programmed, we compared the calculation results of Eq. (10) from Python with those of numerical simulations in Modelica. Modelica is an equation-based modeling language used for scientific simulations across various domains. Building simulation is one of the growing applications of Modelica [40], [41]. Using a Modelica model is appropriate for verifying the correctness of an analytical equation, as it enables the reproduction of an analytical solution under identical settings.

In addition, this verification helped determine appropriate time steps. Because the variables were discretized over a time step, the model assumed that the parameters of the previous time step remain the same during the time step. As such, various time steps were tested: 60, 30, 15, and 3 min. In Modelica, a differential/algebraic system solver is used, where a time step is considered as a variable and determined by the solver.

### 2.2.1. Building settings and boundary conditions

For verification purposes, a two-zone model was set up. The model featured two identical rooms, each with dimensions of 5 m × 5 m × 4 m, as illustrated in Figure 4. The settings and conditions applied in the calculations can be found in Table 1. All cases were calculated over a 24-hour period.
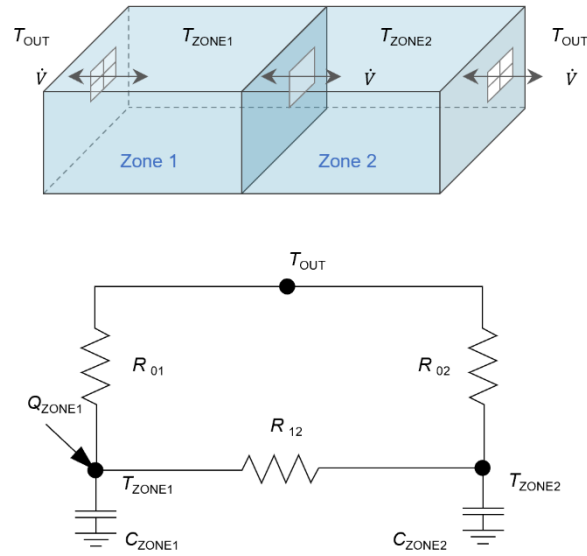
Figure 4. Two-zone 3R–2C model geometry description and analogous circuit diagram

Table 1. Building settings and boundary conditions

| Description | Value | Unit |
|---|---|---|
| Density of air | 1.20 | [kg/m³] |
| Specific heat capacity of air | 1000.00 | [J/kg-K] |
| Zone width × length × height | 5×5×4 each | [m³] |
| Surface area of building envelope | 85 each | [m²] |
| Surface area of internal wall | 20 | [m²] |
| Area of window of each zone | 2.72 | [m²] |
| Area of effective window | 1.173232 | [m²] |
| Overall U-value of exterior wall | 0.15 | [W/m²-K] |
| Overall U-value of interior wall | 0.30 | [W/m²-K] |
| Heat storage | 2,400,000 | [J/K] |
| Internal heat gain (when applicable) | 325.00 | [W] |
| Infiltration rate (when closed) | 0.005 | [m³/s] |
| Natural ventilation rate (when opened) | 0.2 | [m³/s] |

### 2.2.2. Parameters: internal heat gain and window status

The internal heat gains and window status modes applied to the test model are listed in Table 2. For the closed window scenarios (Cases 1 and 2), an infiltration rate of 0.005 m³/s was used. For the open window scenarios (Cases 3 and 4), an increased airflow of 0.2 m³/s was applied. In all scenarios, the air was assumed to flow from the outdoors to Zone 1, from Zone 1 to Zone 2, and then from Zone 2 back to the outdoors. Solar heat gain was not considered. Instead, heat gains from three occupants were considered in Cases 2 and 4 to assess the influence of internal heat gains. A Modelica model for Case 4 is illustrated in Figure 5, and the outdoor air temperature profile used for this test is presented

in Table 3. With temperatures ranging from 15°C to 27°C, this temperature profile represents a day when natural ventilation could serve as a cooling source throughout the day.

Table 2. Internal heat gain and window status of the test cases

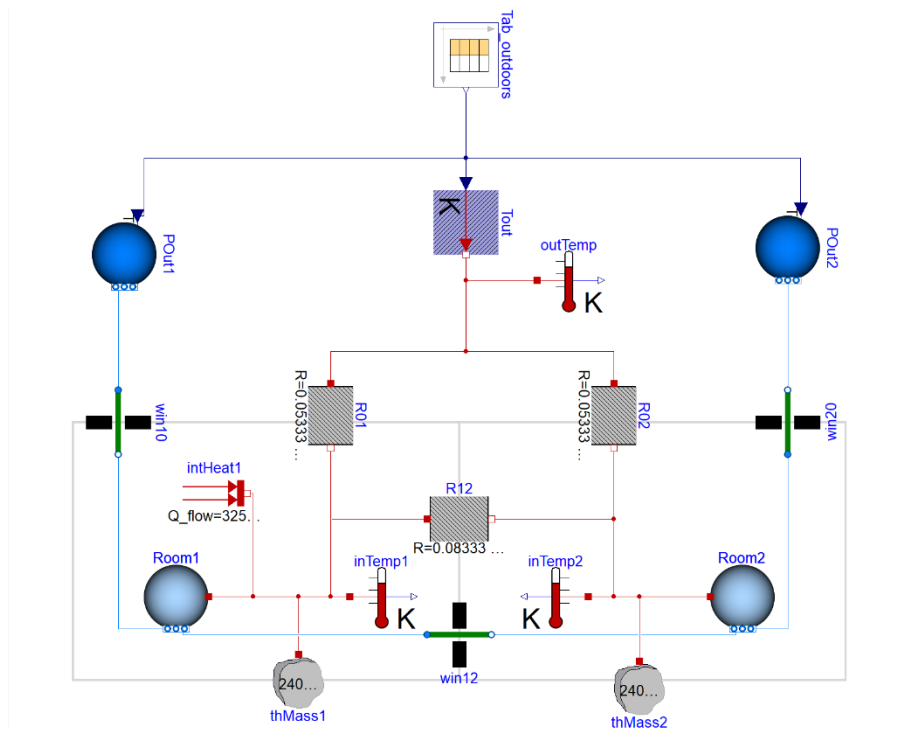| Test case | Internal heat gain | | Window status |
| | Zone 1 | Zone 2 | |
| --- | --- | --- | --- |
| **Case 1** | 0 W | 0 W | Closed (0.005 m³/s) |
| **Case 2** | 325 W | 0 W | Closed (0.005 m³/s) |
| **Case 3** | 0 W | 0 W | Open (0.2 m³/s) |
| **Case 4** | 325 W | 0 W | Open (0.2 m³/s) |



Figure 5. Modelica model (Case 4, in which intHeat1 injects heat to Room 1) of the two-zone model shown in Figure 4.

Table 3. Hourly outdoor temperature of a day used for test cases

| Time of day | 0 | 1 | 2 | 3 | 4 | 5 | 6 | 7 | 8 | 9 | 10 | 11 |
| --- | --- | --- | --- | --- | --- | --- | --- | --- | --- | --- | --- | --- |
| **Temperature (°C)** | 20.6 | 16.5 | 16.1 | 15.6 | 15.6 | 15.0 | 15.0 | 16.7 | 18.3 | 20.6 | 22.2 | 23.3 |
| **Time of day** | 12 | 13 | 14 | 15 | 16 | 17 | 18 | 19 | 20 | 21 | 22 | 23 |
| **Temperature (°C)** | 23.9 | 25.0 | 25.6 | 26.7 | 26.7 | 26.7 | 26.1 | 25.6 | 22.8 | 22.2 | 21.1 | 21.1 |

### 2.2.3. Comparison between $n$R–$m$C model and Modelica calculation results

The root-mean-square error (RMSE) of Zone 1 air temperature was calculated for each case to quantify the agreement between the models. The RMSE indicates the average deviation of the two datasets calculated using Eq. (11), where $x$ is a value in dataset $X$, and $y$ is in dataset $Y$, each having $n$ elements.

$$RMSE = \sqrt{\frac{\Sigma_{i=1}^{n}(x_i - y_i)^2}{n}} \tag{11}$$

As shown in Figure 6, the $n$R–$m$C model and the Modelica calculation results showed a good agreement. Using shorter time steps in the $n$R–$m$C model reduced the discrepancy between the two sets of calculations. A higher level of agreement with shorter time steps was expected because any variables in each parameter were assumed constant throughout the time step. The increased airflow rates resulted in significant differences in RMSE between Case 1 (0.005 m³/s) and Case 3 (0.2 m³/s), as well as between Case 2 and Case 4. This was because the time constant $\tau^*$ in Eq. (7) became smaller for a case with an airflow of 0.2 m³/s than the one with an airflow of 0.005 m³/s. Contrary to the effect of airflow, the influence of internal heat gain on the RMSE was marginal, as seen when comparing Case 1 (0 W) to Case 2 (325 W), and Case 3 to Case 4. Considering that a 10-minute interval is commonly used for general building simulation in EnergyPlus, and recognizing the relatively lower RMSE at 3 and 15 minute time steps, we opted for a 10-minute time step for the subsequent tests in this study.
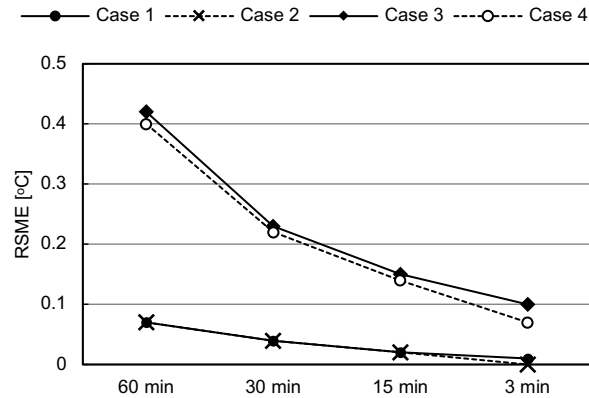


Figure 6. RMSE plot of Zone 1 air temperature of the multi-zone test cases with different time steps against Modelica simulation

## 2.3. Controller for dynamic window operations

### 2.3.1. Control algorithm and preliminary tests

Using the analytical solution derived in the previous sections, we developed a control algorithm aimed

at maintaining the predicted indoor air temperature at the lowest possible level during the summer. To predict the room temperature for the subsequent time step, the algorithm requires inputs such as the present room temperature ($T_{\text{rm},i}$), the temperature of adjacent zones ($T_i^*$) as defined in Eq. (8), the time constant ($\tau_i^*$) as defined in Eq. (7), and the thermal resistances for both open and closed cases ($R_{\text{opened},i}^*$ and $R_{\text{closed},i}^*$) as defined in Eq. (6). Given our focus on the cooling season, a heating setpoint was not integrated into the algorithm. As windows can be either opened or closed, the algorithm first predicts the temperature for the subsequent time step under both conditions using Eqs. (12) −(13). It then compares the two predicted temperatures and selects the window action (either open or close) that leads to the lower temperature, as outlined in Eq. (14).

$$
\begin{aligned}
f\big(T_{\text{rm},i}, T_i^*, Q_{\text{rm},i}, \tau_{\text{opened},i}^*, R_{\text{opened},i}^*\big) \\
= T_{\text{rm},i}\, e^{-\frac{t}{\tau_{\text{opened},i}^*}} + \big(T_i^* + R_{\text{opened},i}^*\, Q_{\text{rm},i}\big)\left(1 - e^{-\frac{t}{\tau_{\text{opened},i}^*}}\right),
\end{aligned} \tag{12}
$$

$$
f\big(T_{\text{rm},i}, T_i^*, Q_{\text{rm},i}, \tau_{\text{closed},i}^*, R_{\text{closed},i}^*\big) = T_{\text{rm},i}\, e^{-\frac{t}{\tau_{\text{closed},i}^*}} + \big(T_i^* + R_{\text{closed},i}^*\, Q_{\text{rm},i}\big)\left(1 - e^{-\frac{t}{\tau_{\text{closed},i}^*}}\right), \tag{13}
$$

where
$R_{\text{opened},i}$: thermal resistance when window is opened per Eqs. (2) and (6) [K/W],
$R_{\text{closed},i}$: thermal resistance when window is closed per Eqs. (2) and (6) [K/W],
$\tau_{\text{opened},i}$: time constant when window is opened [s],
$\tau_{\text{closed},i}$: time constant when window is closed [s],

and the subscript $i$ of each variable means that the variable is of the $i^{th}$ time step.

$$
T_{\text{rm},i+1} = min\left(f\big(T_{\text{rm},i}, T_i^*, Q_{\text{rm},i}, \tau_{\text{opened},i}^*, R_{\text{opened},i}^*\big), f\big(T_{\text{rm},i}, T_i^*, Q_{\text{rm},i}, \tau_{\text{closed},i}^*, R_{\text{closed},i}^*\big)\right). \tag{14}
$$

When using this algorithm for simulation purposes, the input variables ($T_{\text{rm},i}, T_i^*, q_i, \tau_i^*$, and $R_i^*$) should be calculated from the $i^{th}$ time step. For a smart building application, certain variables including $T_{\text{rm},i}$, $T_i^*$, and $q_i$, can be obtained by sensors. However, accessing other variables might be challenging. In such cases, a trained model that emulates the building's thermal behavior can be used to determine these data types.

### 2.3.2. Preliminary test for the comparison among the different operation modes for two rooms with different internal heat gain schedules

To demonstrate how the window scheduler algorithm works for two thermally connected zones that have different internal heat gain schedules, we conducted a preliminary test with the two-zone model used in Figure 4. With rather limited settings. including constant airflow rates and no solar radiation, the test aimed to reveal the benefit of adopting dynamic operations guided by the controller.
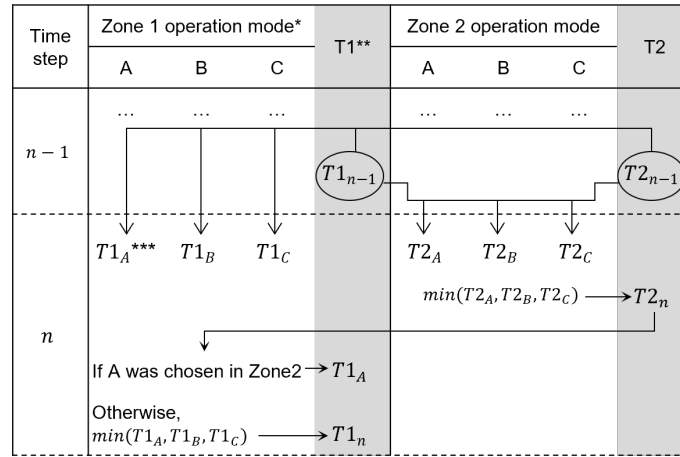
Two exterior openings, one for each zone, and one interior opening between the zones were set up. For test purposes only, airflow rates for cross ventilation, single-sided ventilation, and infiltration

were chosen as follows. When all openings are open, cross ventilation occurs from outdoors to Zone 1, from Zone 1 to Zone 2, and then from Zone 2 to the outdoors at a rate of 0.2 m³/s. When all but the internal opening was open, each room was assumed to have fresh air at a rate of 0.05 m³/s through single-sided ventilation. When three openings were closed, infiltration of 0.005 m³/s was applied. In practice, these flowrates are subject to change, not only with wind direction and speeds, but also with various window types (awning, casement, sliding, etc.), arrangements (two windows arranged vertically, horizontally, etc.), and the airtightness of buildings. These factors can be modeled in a more detailed simulation set-up. The outdoor temperature profile of Table 3 was applied. Heat rate schedule from occupancy are outlined in Table 4.

Table 4. Internal heat gain schedule assumption for the two rooms

|  | 0:00 – 7:59 | 8:00 – 11:59 | 12:00 – 13:29 | 13:30 – 17:59 | 18:00 – 23:59 |
|---|---|---|---|---|---|
| **Zone 1 [W]** | 50 | 300 | 150 | 300 | 50 |
| **Zone 2 [W]** | 65 | 390 | 195 | 390 | 65 |

For both rooms, we tested four window operation modes: always closed (mode 1), always opened (mode 2), operated by outdoor air temperature (mode 3), and operated by the algorithm (mode 4). In mode 3, all three windows were open when the outdoor air temperature was 25 °C or lower and were closed otherwise. Since openings were operated by the outdoor temperature, the three openings were operated identically. On the contrary, in mode 4, the algorithm provided an opening schedule tailored to each window, resulting in cross ventilation, single-sided ventilation, or no ventilation as desired. As illustrated in Figure 7, at each time step, the hypothetical temperatures of cross/single-sided/no ventilation were computed. If a window action was beneficial to one zone but not the other, we gave priority to Zone 2's thermal comfort given its relatively greater internal heat gains than Zone 1.

| Time step | Zone 1 operation mode* | | | T1** | Zone 2 operation mode | | | T2 |
|---|---|---|---|---|---|---|---|---|
| | A | B | C | | A | B | C | |
| $n-1$ | … | … | … | $T1_{n-1}$ | … | … | … | $T2_{n-1}$ |
| $n$ | $T1_A$*** | $T1_B$ | $T1_C$ | | $T2_A$ | $T2_B$ | $T2_C$ | |

$$min(T2_A, T2_B, T2_C) \longrightarrow T2_n$$

If A was chosen in Zone2 → $T1_A$

Otherwise,
$min(T1_A, T1_B, T1_C) \longrightarrow T1_n$

\* Operation mode
A: Cross ventilation (all openings are open)
B: Single-sided ventilation (all but internal opening are open)
C: No natural ventilation (all openings are closed)

\*\*T1 and T2 are the Zone1 and Zone 2 temperatures at the end of each time step based on the selected operation mode determined during the time step.

\*\*\* $T_A$, $T_B$, and $T_C$ are the hypothetical zone temperatures of modes A, B, and C calculated based on the previous zone conditions.

Figure 7. Mode 4 operation logic.

The graphs in Figure 8 compare the air temperatures of Zone 1 and Zone 2 under different window operation modes, for hours 72-144 of a 144-hour simulation period. The gray lines represent the zone air temperature of mode 1 when the windows are always closed. Although the initial temperature was the same as for the other three operating modes, the temperature when windows are always closed increases at a rate determined by heat gains and thermal storage and reaches steady-periodic equilibrium after about three days of simulation period. These lines suggest that both rooms need cooling throughout the entire simulation period even if the outdoor temperature (the black dashed line) is lower than the desired temperature, which this case sets to 25 °C.

The red lines show the zone air temperature of mode 2 when the windows are always open regardless of the outdoor temperature. This mode results in approximately six hours of over-warming in Zone 1 and seven in Zone 2 each day.

The yellow lines represent the mode 3 indoor temperature results when windows are operated based on the outdoor air temperature. The windows are closed between 1 PM and 7:15 PM when the outdoor is warmer than 25 °C, as denoted by the yellow bar graph below the temperature graphs. Although windows are closed to block the flow of overly warm outdoor air, there are still times when the indoor temperature exceeds the comfort threshold owing to the internal heat gains and heat stored in the thermal mass.

Finally, in mode 4 when the windows are operated by the algorithm (Eq. (14)), the air temperature in

both zones remains as low as possible (the blue lines). The algorithm yields a unique window schedule for each zone as shown in the blue bar graphs at the bottom of Figure 8. For Zone 1, windows are closed from 7:00 AM to 7:00 PM. Even when the outdoor air temperature is lower than 25 °C in the morning, the algorithm stipulates that windows be closed, preventing a stiff increase in indoor air temperature. For Zone 2, windows are closed from 9:30 AM to 7:00 PM). From 7 PM to 10:15 PM, the algorithm recommends that the internal opening be opened to enable cross ventilation for both zones.
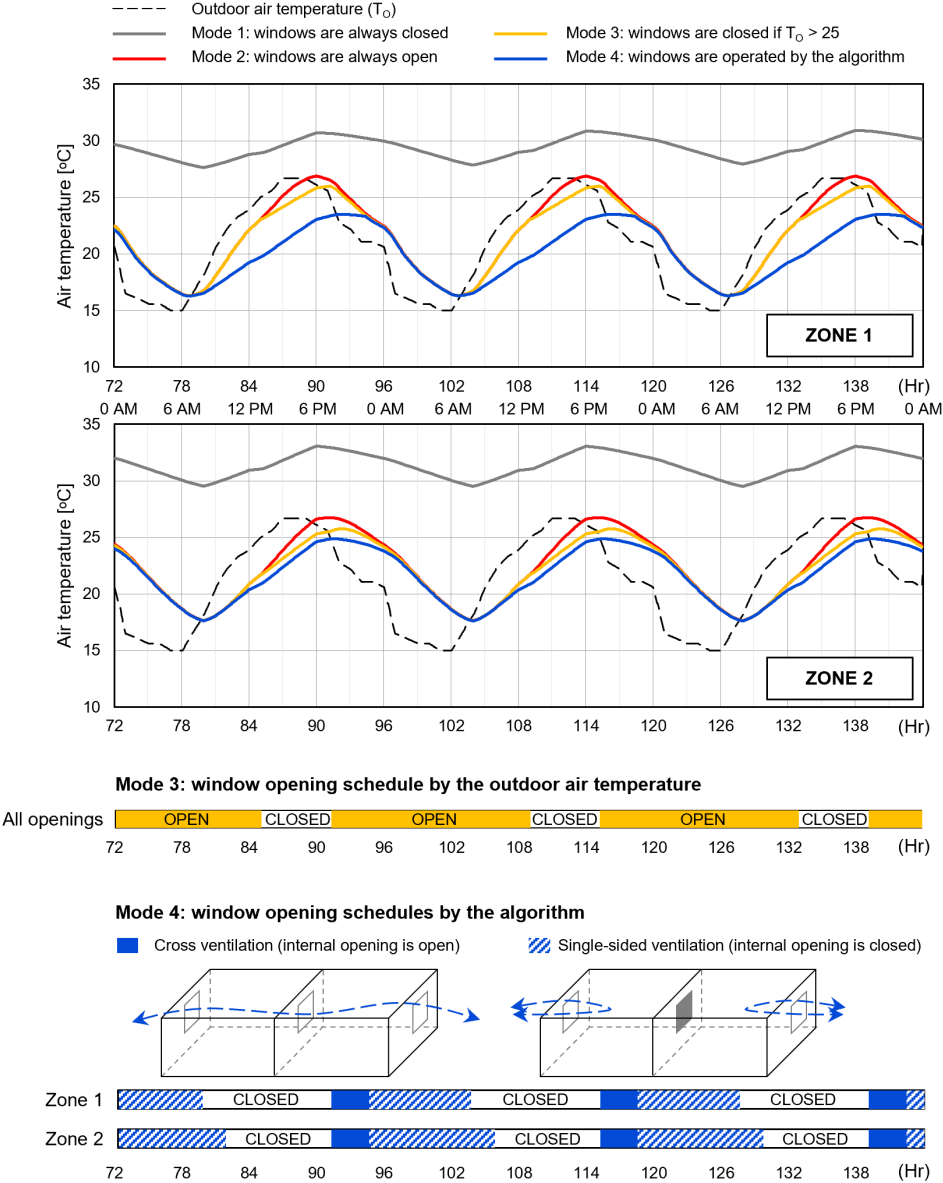


Figure 8. Air temperature of Zones 1 and 2 over three days under the four modes of window operation. The horizontal bar graphs represent the window status (closed or opened) during modes 3 and 4.

The results of these four operation modes show that the conventional window assumptions in building

16

energy simulation may fail to capture the optimal performance of natural ventilation, and that the analytical solution is useful for determining the timely window operation. They also demonstrate that the controller can offer a customized window schedule for each zone depending on its own conditions such as internal heat gains and temperatures of thermally connected zones.

## 3. Case study: Application of window schedule algorithm to an EnergyPlus model

To implement the window scheduler derived from the $n$R–$m$C model, we conducted a case study using the BESTEST "FF600" (where FF stands for free-flow) model provided by ANSI/ASHRAE Standard 140 [42] as our test building. The FF600 model was chosen for its suitability to our objectives: it is utilized to evaluate various computer programs for building energy analysis; its initial settings are relatively straightforward, facilitating the emulation of the $n$R–$m$C model; and its infiltration rate, in the absence of any HVAC system, properly represents a scenario with natural ventilation.

The procedure was as follows: Using Python code, we emulated the test building with the $n$R–$m$C model. Next, we implemented the window control algorithm to recommend window operations at each time step, considering the building's mass and flow rates. To execute the Python code, several input values, such as solar radiation, infiltration, and temperature boundary conditions, were required. To obtain these inputs, we simulated the test case in EnergyPlus and used its outputs as inputs for our test model. The code then generated the optimal window schedule targeting the lowest possible room temperature during the summer. We tested this in Fresno (CA), Phoenix (AZ), Houston (TX), and Denver (CO) of the United States. After establishing the optimal window schedule for each climate, we sought to validate if the indoor temperature indeed decreased when applying these schedules. To confirm this, we conducted further EnergyPlus simulations, applying these window schedules, and then compared the results.

### 3.1. The FF600 model and test parameters

The input data file (IDF) of the FF600 model (Figure 9) for the EnergyPlus simulations was downloaded from the EnergyPlus website [43]. The FF600 model has an infiltration rate of the FF600 model is 0.5 ACH. To investigate the impact of different airflow rates, we applied 0.5, 1, 2, 4, and 8 ACH. While ventilation rates in reality constantly fluctuate, using fixed yet diverse values of airflow rates help understand the interplay between various climates, airflow rates, heat capacities, and window schedules. We utilized the thermal capacitance multiplier (TCM) feature of EnergyPlus to introduce varying amounts of thermal mass to the room. This feature facilitates the examination of different internal thermal masses by multiplying the total thermal storage of the zone's air volume. For example, a TCM of 20 was used by Hong and Lee [44] to test their physics-based model in

17

EnergyPlus. To select the test TCM values, we assume that a concrete mass with the same size of floor ($8 \times 6 = 48$ m²) and a thickness of 0.04 m, which has a heat capacity of approximately 4,608 kJ/K. This is approximately 30 times the room air heat capacity. We use TCMs of 1, 10, 25, and 50 in the room to check the augmented effect of various TCMs, although a TCM of 50 can be unrealistic.
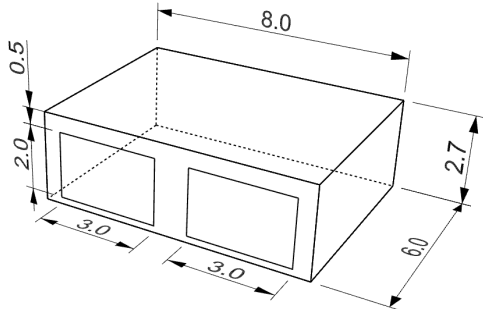


Figure 9. BESTEST FF600 geometry. The dimensions are in meters.

As previously stated, tests were done under four climates: Fresno (CA), Phoenix (AZ), Houston (TX), and Denver (CO). The control algorithm provided window scheduling recommendations for each climate, and validation of the recommended window schedule was tested for the Fresno case. The simulation period was from July 1 to July 15, with the mean diurnal outdoor air temperature illustrated in Figure 10.
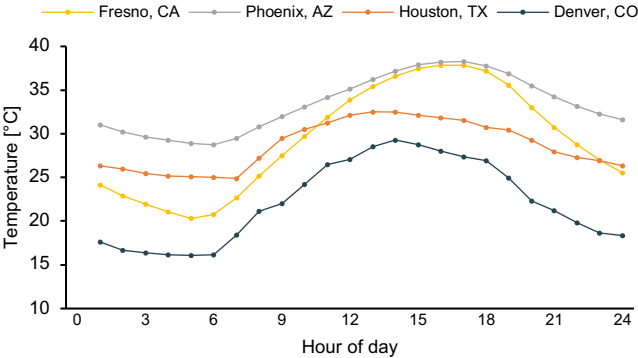


Figure 10. Mean hourly outdoor air temperature of Phoenix (AZ), Houston (TX), and Denver (CO) during the simulation period (July 1– 15).

### 3.2. The 7R–7C multi-mass model

Because the FF600 model appears to be a single zone, one might consider constructing it with a 1R-1C model by consolidating the resistances of various walls and the roof into a unified thermal resistance and applying thermal mass of the envelope to the room zone. However, such simplification neglects the distinct thermal capacities of each construction component. Moreover, considering that these components receive varying amounts of solar radiation based on their orientations, which in

18

turn affects their temperatures, it is insufficient to treat them merely as thermal resistances facing the outdoors. As such, we treated each thermally massive component as an adjacent zone to the primary indoor zone, despite the roof, floor, and four walls not being typical room zones. In essence, this approach transformed this seemingly single zone into a 7R-7C model, as illustrated in Figure 11.
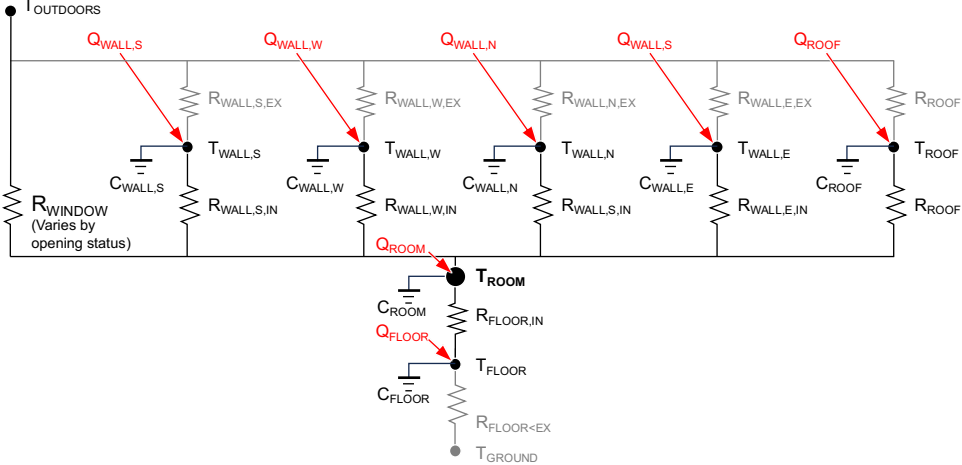


Figure 11. BESTEST FF600 represented as the analogous 7R–7C circuit model. The room node, $T_{ROOM}$, was connected to seven thermal resistors and is influenced by seven thermal storages.

Regarding weather inputs, the outdoor temperature was assigned to the $T_{OUTDOOR}$ node, and the solar radiation received by each building surface was considered in Qs in Figure 11. It is important to note that Qs includes not only the solar radiation on external surfaces but also any solar radiation received by internal surfaces and additional internal heat gains. While wind information could have contributed to a more comprehensive case study, we implemented air change rates of 0.5, 1, 2, 4, and 8 ACH, as justified in Section 3.1. To consider various ventilation rates, $R_{WINDOW}$ from Figure 11 was adjusted according to Eq. (2). When natural ventilation was not factored in, only the base infiltration rates from the initial FF600 model were used in Eq. (2). To align the other boundary conditions of the 7R–7C model to the EnergyPlus model, outputs from the initial run of the FF600 model were extracted and used for the input values for the 7R–7C model, as outlined in Table 5.

Table 5. Source of the required inputs of the 7R–7C model

| Required input of the 7R–7C model | EnergyPlus output of the FF600 model used for the 7R–7C model or calculated values using the FF600 model |
|---|---|
| $T_{OUTDOORS}$ [C] | "Environment:Site Outdoor Air Drybulb Temperature" from the output file |
| $T_{GROUND}$ [C] | "Surface Outside Face Temperature" of the floor surface from the output file |
| $Q_{WALL,N}$, $Q_{WALL,E}$, $Q_{WALL,S}$, $Q_{WALL,W}$, and $Q_{ROOF}$ [W] | The sum of "Surface Inside Face Internal Gains Radiation Heat Gain Rate," "Surface Inside Face Solar Radiation Heat Gain Rate," and "Surface Outside Face Solar Radiation Heat Gain Rate" of each wall or roof from the output file |
| $Q_{FLOOR}$ [W] | The sum of "Surface Inside Face Internal Gains Radiation Heat Gain Rate" and "Surface Inside Face Solar Radiation Heat Gain Rate" from the output file |
| $Q_{ROOM}$ [W] | The sum of "Zone Other Equipment Total Heating Rate", "Surface Window Total Glazing Layers Absorbed Shortwave Radiation Rate" and "Surface Inside Face Internal Gains Radiation Heat Gain Rate" from the output file. |
| Airflow rate ($\dot{V}$ of Eq. **(2)**) [m³/s] | "Zone Infiltration Standard Density Volume Flow Rate" of the room from the output file |
| $C_{ROOM}$ [J/K] | 1.225 [kg/m³] * 1000 [J/K/kg] * volume of the room [m³] * TCM |
| C [J/K] (all C's except $C_{ROOM}$) | Calculated from the "Materials" object of the IDF file |
| R of Eq. **(2)** [K/W] (for all R's) | Calculated based on the "Materials," "Materials:NoMass," "WindowMaterial:Glazing," and "WindowMaterial:Gas" objects of the IDF file where applicable |

### 3.3.   Validation of the model

To confirm the capability of the model to emulate the FF600 model accurately, we conducted year-long simulations for Fresno (CA), even though the case study primarily examines a two-week period. These simulations were then compared with the results from EnergyPlus simulations for validation purposes. Building upon the initial settings outlined in earlier sections, we incorporated additional inputs as specified by [42] in Table 6.

Table 6. Test building settings

| Elements | Type | Value |
|---|---|---|
| **Wall (all sides)** | R-value (without air films) | 1.789 [m²K/W] |
| | R-value (with air films) | 1.944 [m²K/W] |
| **Wall (north)** | Heat capacity | 313.9 [kJ/K] |
| **Wall (south, excluding windows)** | Heat capacity | 139.5 [kJ/K] |
| **Wall (east and west)** | Heat capacity | 342.7 [kJ/K] |
| **Roof** | R-value (without air films) | 2.992 [m²K/W] |
| | R-value (with air films) | 3.147 [m²K/W] |
| | Heat capacity | 872.2 [kJ/K] |
| **Floor** | R-value (without air films) | 25.253 [m²K/W] |
| | R-value (with air films) | 25.374 [m²K/W] |
| | Heat capacity | 936.0 [kJ/K] |
| **Windows** | R-value (with air films) | 0.333 [m²K/W] |
| | Shading coefficient | 0.907 |
| | Solar heat gain coefficient | 0.789 |
| **Infiltration** | Airflow rate | 0.5 ACH |
| **Internal load** | | 200 W continuous |
| **Soil temperature** | | 10 °C continuous |

Figure 12 presents a comparison between the outcomes of the nR-mC model and those obtained from EnergyPlus. For improved readability, the graph displays only the first two weeks in January, April, July, and October. The correspondence between the two sets of results is strong, as indicated by a high correlation coefficient of 0.964 and an R-squared value of 0.982, demonstrating good alignment.

Potential discrepancies between the results may have stemmed from the differing approaches to convective heat transfer and the assignment of materials to thermal nodes. EnergyPlus incorporates multiple algorithms to account for internal and external convection, whereas our model employs a more heuristic approach to approximate convective effects using internal and external air films. Additionally, EnergyPlus assigns each layer of a wall, whether thermally massive or lightweight, to one or two nodes, whereas our model aggregates a structural material into a single node.
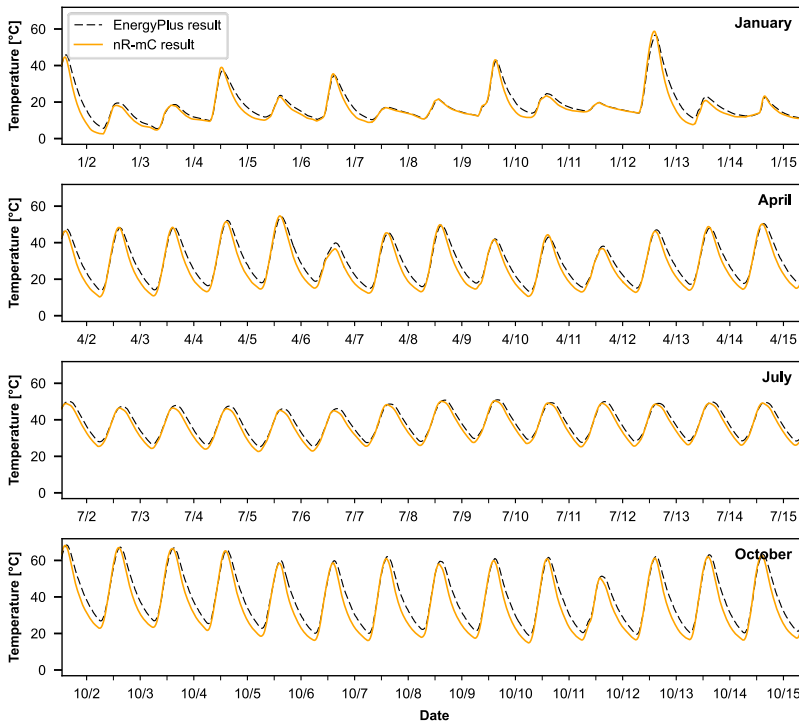
Figure 12. Validation results with BESTEST FF600: EnergyPlus Vs. nR-mC model.

## 4. Results

### 4.1. *Window schedule recommended by algorithm*

At each time step, the algorithm provided a window status recommendation (1 for 'open' and 0 for 'close'). By averaging hourly recommendations across the two-week simulation period, we generated daily operation schedules. The averaged schedules for the Fresno case are shown in Figure 13.
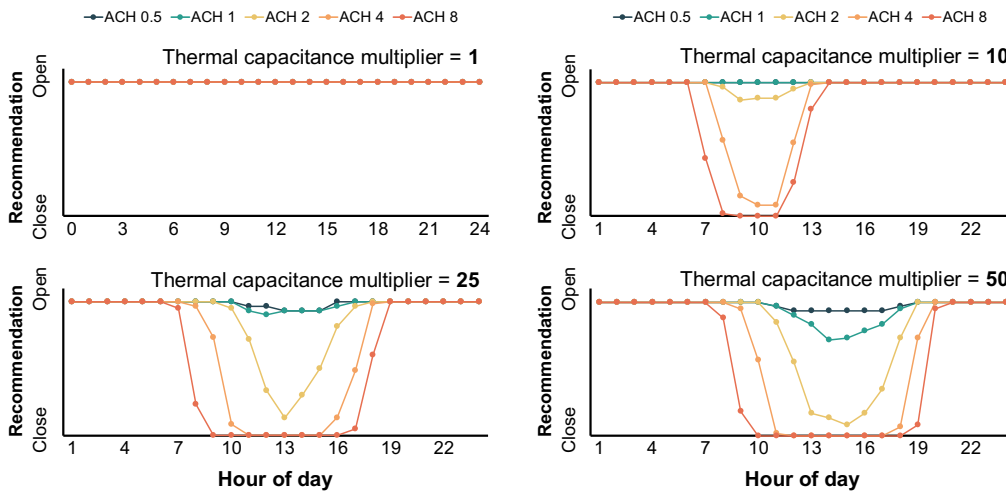


Figure 13. Diurnal averaged window operations optimized under various ACH and TCM scenarios during the

The results from the Fresno case suggest that the windows should remain open when the TCM is 1, regardless of the ACH values. As the TCM increased, the algorithm modified its recommendation, suggesting that closing windows at certain times of the day might be beneficial. The recommendations also varied based on ACH. With higher airflow rates and heavier mass, there were longer durations when closing windows was advised. For example, the window schedules for Fresno at an ACH of 8 (~0.3 m³/s) were determined as follows:

1) Windows should be always opened (schedule recommended for TCM 1),
2) Windows should be closed during 6:30–13:00 but opened for the rest of the time (recommended for TCM 10),
3) Windows should be closed during 7:30–18:30 but opened for the rest of the time (recommended for TCM 25), and
4) Windows should be closed during 8:30–19:30 but opened for the rest of the time (recommended for TCM 50).

The window schedules recommended for the remaining three climates are shown in Figure 14. Under TCM 1, the control algorithm suggested keeping windows open for most of the time for all climates. However, as the TCM value increased, distinctions in window schedules become evident. In cooler climates like Denver, relatively longer durations for window closure were recommended, compared to warmer climates like Phoenix. Similar to the Fresno case, higher TCM and ACH values corresponded to prolonged periods of window closure, particularly during the early morning hours before the room began to warm up.
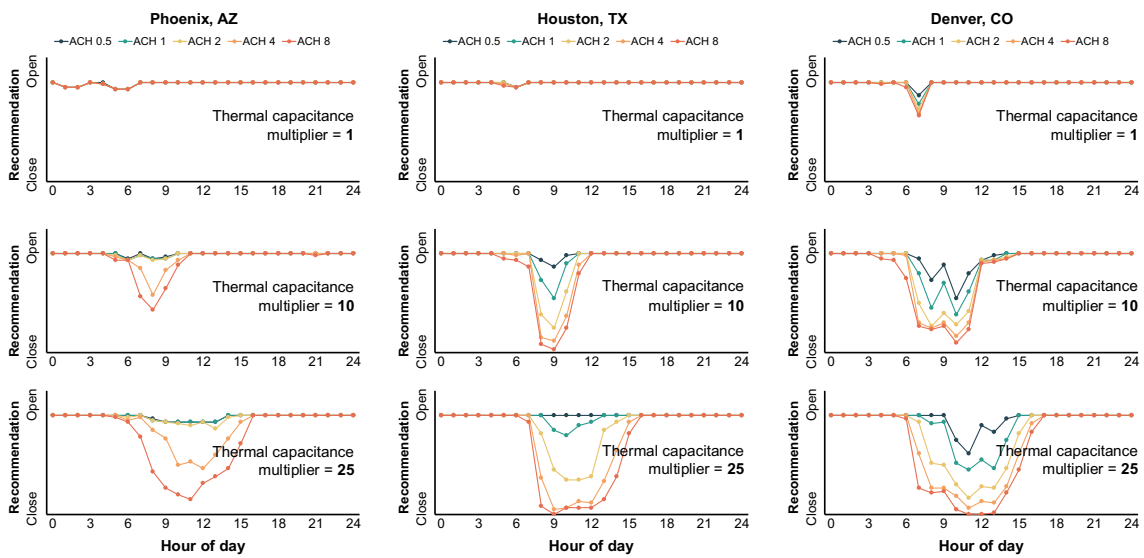


Figure 14. Diurnal averaged window operations recommended under various ACH and TCM scenarios during

the simulation period (July 1–July 15) in various climates.

The schedules outlined above might not guarantee thermal comfort, regardless of their effectiveness in reducing indoor temperatures, especially when the outside weather is hot. Operating a home or office entirely in passive mode during the specified test period might compromise occupants' thermal comfort in warmer climates like Phoenix even with thoughtfully planned window schedules. Thus, occupants might consider adopting this operational strategy during milder times. Nevertheless, as examined in Refs. [45]–[47], using strategic window operations can still be advantageous from a resilient cooling perspective, helping to mitigate extreme indoor temperatures during power disruptions or equipment failures amid heatwaves.

## 4.2. *Cooling effect of the recommended operation schedules*

To validate that these window operations would effectively lower the indoor air temperature, we ran the FF600 EnergyPlus simulations again with the changes in operation schedules, as illustrated in Figure 15. Fresno weather data were used. For each TCM, we applied four window schedules as follows:

1) [Base case] Windows are always opened (schedule recommended for TCM 1),
2) Windows are closed during 6:30–13:00 but open for the rest of time (recommended for TCM 10),
3) Windows are closed during 7:30–18:30 but opened for the rest of the time (recommended for TCM 25), and
4) Windows are closed during 8:30–19:30 but opened for the rest of the time (recommended for TCM 50).

The window operation with no control (always open) was set as a base case and compared with the other three schedules.
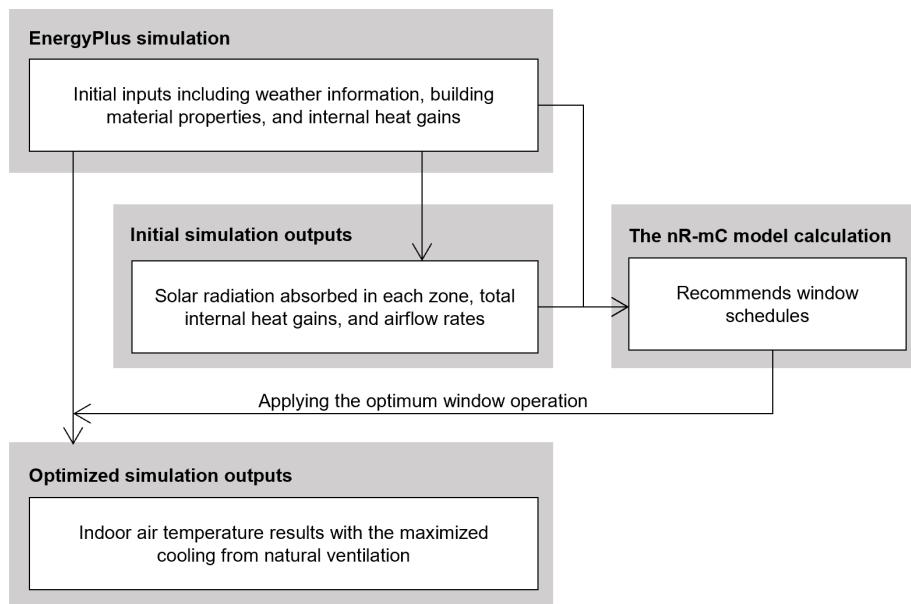
Figure 15. Validation process of the window schedules recommended by the control algorithm.

To compare the resulting room air temperatures, we calculated the deviations in the minimum, mean, and maximum room air temperatures from the base case, as illustrated in Figure 16. The *x*-axis denotes the four window operations, corresponding to the schedules recommended for TCMs of 1, 10, 25, and 50 by the control algorithm. Negative values in the *y*-axis indicate that the room air temperature under the operation schedule was lower than that of the base case, making it more optimal. With TCM of 1, the lowest minimum, mean, and maximum room air temperatures were achieved in the base case, consistent with the algorithm's recommendation. For the window closure schedule of 6:30–13:00, there was no notable change in the room temperature from the base case, albeit with a slight increase. However, when windows were closed for extended periods (7:30–18:30 and 8:30–19:30), the peak room temperature increased by up to 8 K.

For cases with TCMs of 10, 25, and 50, the room temperature decreased under the schedules specifically recommended for their own cases. When TCM was 10, approximately equivalent to adding a third of the floor-sized concrete mass with a thickness of 0.04 m indoors, the influence of the recommended window operation was small. Nevertheless, the recommended operation (6:30–13:00) still offered the coolest indoor environment. Closing windows 7:30–18:30 led to the lowest indoor air temperature for the case with TCM 25, and 8:30–19:30 for the case with TCM 50.
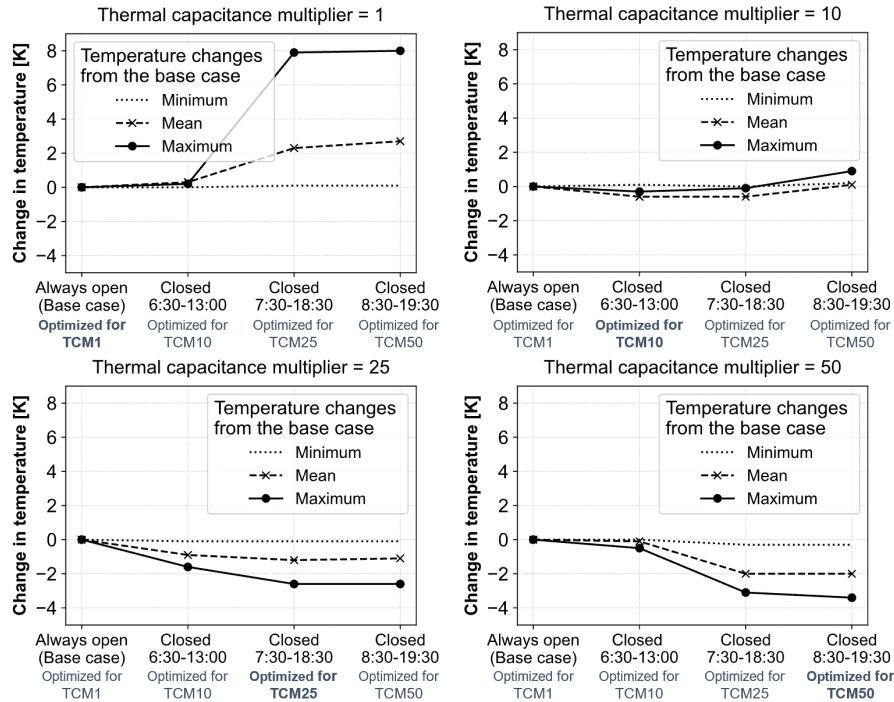
25

Figure 16. Changes in the minimum, mean, and maximum room air temperatures with four different operation schedules during the simulation period (July 1– 15).

The results confirm that the control algorithm, derived from the thermal circuit model, effectively determines a window schedule for maintaining indoors as cool as possible through passive cooling . As highlighted in the recent research about resilient cooling [47]−[48], lowering indoor temperature can be particularly beneficial in scenarios where HVAC systems are either absent or malfunctioning. Furthermore, the results indicate that inappropriate window operation can negatively impact indoor thermal comfort, which underscores the importance of strategic scheduling. For example, window schedules such as being closed from 8:30 to 19:30 in a case with TCM 1, or remaining open throughout for TCM 25 or above, can be counterproductive. Additionally, the reduced temperatures resulting from the optimized window operation schedules suggest the potential for cooling energy savings when the algorithm is integrated with HVAC systems. However, the control algorithm (Eq. (14)) requires adjustments to ensure compatibility with thermostat settings. It should not only predict temperatures for open or closed window scenarios but also take into account the thermostat setpoint, and accommodate scenarios where the air conditioning is either off or on with the windows closed. The inclusion of the mixed-ventilation mode where AC is on while window is also open, though typically not energy-efficient nor recommended, should also be determined by a user. Additional savings could be achieved by combining the window algorithm and thermostat control as researched by [49].

## 5. Discussion

For the proposed algorithm to function optimally, it requires several key inputs, including temperatures of adjacent zones, solar heat gains, and infiltration rates. If additional zones, such as corridors or rooms on different floors, are to be added and inter-zonal airflow becomes a factor, the needs for integration with existing simulation tools or advanced sensing systems increase. Therefore, we suggest two potential applications where the proposed controller can be integrated.

The first potential application is the implementation of the algorithm with simulation programs such as EnergyPlus and Spawn of EnergyPlus (or Spawn) [50]. As illustrated in Figure 15, the optimal window schedule presented in this study was computed outside of the EnergyPlus environment, using the initial outputs from EnergyPlus simulation results. During this process, hourly variations in several parameters, including the exterior and interior convective heat transfer coefficients determined at each time step by various surface convection algorithms within EnergyPlus, were modeled as constants in the $n$R–$m$C model. In addition, the diurnal window schedules were averaged over a two-week period. As a result, while the hourly recommended schedule might be optimal for most days, it may not be for certain days. If the algorithm were to be embedded directly within the EnergyPlus solver or the Modelica Buildings Library [41], [51], the recommended window status could be updated in each control time step. This would then be based on the inherent parameters of either the EnergyPlus or Spawn variables, eliminating the need to couple the Python codes to each program.

A practical application in this context is the Energy Management System (EMS) feature within EnergyPlus. The EMS allows users to use the output variables as sensors to determine the actions of an EMS actuator (e.g., window operation). As the EMS sensors use output variables from the current time step, a function is needed to determine the window status in a manner that ensures the zone air temperature in the subsequent time step remains as low as possible. Equation (14) enables this by monitoring the corresponding output variables, as shown in Figure 11. This approach does not require complex matrix exponentials for multi-zone calculations or an external program that must be coupled to EnergyPlus. Instead, the following pseudocode can be implemented:

**EMS pseudo code**

```
IF (T_next when opened) < (T_next when closed),
SET window to open,
ENDIF;
```

where $T_{\text{next when opened}}$ and $T_{\text{next when closed}}$ can be computed using Eqs. (12)–(13). In addition, a separate EMS object can be set up for another zone, as shown in Figure 8.

Second, the proposed model and control algorithm could offer versatile applications in smart homes,

potentially enhancing both user comfort and energy efficiency. For example, occupants could set up a predetermined window schedule based on weather forecasts, which would guide them on the best times to open or close manually operated windows. Building managers in schools or offices can provide users with daily or weekly guidelines for window schedules, such as those shown in Figure 13 and Figure 14. This guidance would help occupants understand specific recommendations, such as closing windows from 10 to 12 and 2 to 6 on the days they are in the building. In homes, residents might be unable to adjust windows due to being away for work or during nighttime sleep. In these situations, they should weigh the implications of a constant schedule over an extended period and then decide on the most advantageous action. They might set up a duration, for example, 8 hours. If the algorithm recommends closing windows for 75% of that 8 hour and opening them for only the remaining 25%, a user might choose to keep them closed. Another way is to apply a constant window action variable throughout the 8-hour period in the calculation process and predict temperatures for both scenarios to determine the better window operation.

Knowledge of the optimal schedule in advance can also be applied to various home assistant systems capable of automating windows operations, working in combination with a user's preferred temperature setting. When a building is equipped with a window system controllable through a customizable algorithm, the window system can dynamically adjust window operations in response to the current conditions by accessing real-time weather data. The automated control through the algorithm potentially offers enhanced performance, as it continually adjusts based on the latest data, ensuring optimal indoor temperatures. Moreover, further energy savings could be achieved by integrating an air conditioning schedule with the real-time adjustment.

To implement the window control algorithm into such advanced technologies, there are several prerequisites. First, the smart building needs access to real-time weather conditions, including ambient temperature, solar radiation, and wind speed (or more direct measurements from air velocity sensors). The acquisition of these environmental data can be achieved through local weather stations or smart home devices. Another, more challenging, prerequisite is to identify a set of building parameters and variables, including the building's material properties, solar and internal heat gains, infiltration and ventilation rates, and temperatures of the major structure (i.e., exterior wall or floor). Because it would be difficult and likely expensive to measure and calibrate such values directly from sensors, machine learning algorithms can be utilized to fit data from smart meters and smart thermostats to models comparable to Eq. (10), as proposed by Lee and Zhang [52]. Moreover, this would also require measurement of the temperature response of the building to open windows, as open windows change the thermal resistance, as expressed in Eq. (2).

The control algorithm presented in this study is intentionally designed to generate window schedules that prioritize the lowest room air temperature at each time step. This focus was due to our primary

interest in the summer period. However, for a longer duration, this strategy might lead to indoor air temperatures falling below the comfortable range, potentially increasing heating energy consumption and reducing the benefit of passive heating. In addition, while not addressed in the case study, a potential issue of short cycling could arise in which windows are impractically recommended to close and open within short intervals. Therefore, if assessing the whole year performance and maintaining a specific frequency for window operation become important, additional conditions would need to be added into Eq. (14).

In reality, ventilation rates from natural ventilation or infiltration are never constant. The decision to utilize constant airflows (ACH 0.5−8) in our case study was primarily aimed at clearly demonstrating the influence of ventilation rates on window schedules. However, when integrating the window controller into a simulation process or a smart home system, additional considerations arise. For simulation purposes, one can readily substitute the ventilation rate, $\dot{V}$, in Eq. (2) with the revised resistance reflecting the time-dependent flow rate. This can be achieved using the EnergyPlus EMS function discussed earlier. In the context of smart home applications, one could utilize hourly weather forecasts to estimate flow rates for the day using one of the established empirical flow rate models. These empirical models include ASHRAE's method [53], which considers 'local shielding classes,' building height, ambient temperature, and wind speed. Another method by Swami and Chandra [54] takes into account window orientations, wind direction, and window speed for flow rate prediction. Alternatively, some might use sensors to obtain more precise measurements of ventilation rates. Measurements from air velocity or air pressure sensors near any openings can be directly used for flow rate calculation. Indoor carbon dioxide sensors can also be used to estimate flow rate based on several factors including the number of occupants and opening size [55]. These refined values can then be used to update Eq. (2).

## 6. Conclusions

We proposed an optimization algorithm to determine a window operation schedule by developing an analytical $n$R–$m$C model for multi-zone or multi-mass buildings. If various constructional components of a single-zone building have different thermal mass, the room should be considered as a multi-zone as demonstrated by the 7R-7C model from the case study. We validated the proposed model and algorithm, and demonstrated its applicability to an existing simulation tool, EnergyPlus. The achievements and findings are summarized as follows:

- The $n$R–$m$C thermal circuit model was developed and validated against a Modelica model. The circuit model successfully represented the thermal behavior of a two-zone (3R–2C) model with internal heat gains and airflow rates.
- Using the $n$R–$m$C model, the window schedule algorithm recommended one of the two window

operations (open or closed) at each time step that would lower the temperature in the subsequent time step. The algorithm was tested with a two-zone (3R–2C) model and demonstrated the potential advantage of such dynamic window operations. The algorithm was able to recommend window operation schedules customized for each zone depending on the internal heat gains and airflow passage. The timing of window operation greatly influenced the indoor air temperature, demonstrating the significance of strategic window operations to maximize the cooling effect from natural ventilation.

- The implementation of the algorithm to a case study of ANSI/ASHRAE Standard 140 demonstrated the validity and applicability of the proposed algorithm. Using a 7R–7C model to emulate the FF600 model, the algorithm recommended optimized window operation schedules depending on various ventilation rates and thermal storage. The recommended operation schedules effectively reduced indoor temperatures during the test period.

Our proposed model and window control algorithm have the potentials for the following applications:

- The thermal circuit model can be used in existing simulation programs, such as EnergyPlus. Because the algorithm uses the output variables from each time step to determine the opening status (opened/closed), it is less challenging and time-consuming than using a more complicated technique, such as machine learning-based algorithms or matrix exponentials. For enhanced accuracy and a more seamless workflow, embedding the model directly into existing simulation tools is recommended, allowing direct access to inherent parameters.
- The model has the potential to be implemented for smart home control. This would require the building to be equipped with various sensors that measure the variables required to compute the control action. In addition, key thermal properties must be measured or calibrated using system identification.

The window algorithm developed in this study adds value to the existing literature about natural ventilation controls, ranging from rule-based operations to heuristic approaches in machine learning. In fact, this physics-based model can be further enhanced with data-driven machine learning techniques to achieve greater energy efficiency in buildings. Such techniques could be particularly beneficial in identifying uncertain and unknown input values for the $n$R–$m$C model. For future research, we aim to implement our model into existing software to examine the effectiveness of dynamic operation at a finer resolution and to apply it to real-world buildings to gain deeper insights into its practical implications and potential challenges.

**Nomenclature**

- $C_n$: heat capacity of thermal mass of Zone $n$ [J/K]

- $T_n$: temperature of Zone $n$ [K]

- $\Delta T_n$: temperature difference between the test room and Zone $n$ [K]

- $R$: thermal resistance accounting for conduction and infiltration [K/W]

- $R_{\text{opened}}$: thermal resistance of a case where window is opened

- $R_{\text{closed}}$: thermal resistance of a case where window is closed

- $Q_n$: internal and solar heat gain rates of Zone $n$ [W]

- $U_j$: overall heat transfer coefficient (U-value, W/m²-K) of the $j^{\text{th}}$ wall [W/m²-K]

- $A_j$: area of the $j^{\text{th}}$ wall [m²]

- $\rho$: density of air [kg/m³]

- $c_p$: specific heat of air [J/kg-K]

- $\dot{V}_n$: airflow rates from a zone $n$ to the test room [m³/s]

## Appendix A.  A step-by-step derivation of the zone temperature at the $(i + 1)^{th}$ time step.

To solve for $T_{\text{rm}}$ from Eq. (9), three cases are examined one step at a time: first, when $T^*$ is a non-zero constant and $Q_{\text{rm}}$ is zero; second, when $T^*$ and $Q_{\text{rm}}$ are both non-zero constants; and then lastly, when they vary at a discrete time step.

**Step 1: $T^*$ is a non-zero constant, and $Q_{\text{rm}}$ is zero.**

Eq. (A. 1) restates the Eq. (9) as a starting point.

$$\tau^* \frac{dT_{\text{rm}}}{dt} = T^* - T_{\text{rm}} + R^* Q_{\text{rm}} \tag{A. 1}$$

With zero internal heat ($Q_{\text{rm}} = 0$),

$$\tau^* \frac{dT_{\text{rm}}}{dt} = \Delta T^* \tag{A. 2}$$

$$\Delta T^* = T^* - T_{\text{rm}}. \tag{A. 3}$$

Because $T^*$ is a constant, differentiating $\Delta T^*$ in Eq. (A. 3) yields

$$\frac{d(\Delta T^*)}{dt} = -\frac{dT_{\text{rm}}}{dt}. \tag{A. 4}$$

Using Eq. (A. 4), we can replace $\frac{dT_{\text{rm}}}{dt}$ with a term of $\frac{d(\Delta T^*)}{dt}$, Eq. (A. 2) changes to

$$\tau^* \left( -\frac{d(\Delta T^*)}{dt} \right) = \Delta T^*$$

$$\ln(\Delta T^*) = -\frac{1}{\tau^*} t + A$$

$$\Delta T^* = e^{\frac{1}{\tau} t + A} = \beta e^{-\frac{1}{\tau} t}, \tag{A. 5}$$

where $A$ is a constant of integration and $\beta$ is the initial $\Delta T^*$ where $t = 0$.

**Step 2: $T^*$ and $Q_{\text{rm}}$ are non-zero constants.**

Next, another case is considered, in which $T^*$ and $q_{\text{rm}}$ are non-zero constants. For this case, a modified form of $\Delta T^*$ from Eq. (A. 5) is taken and then differentiated as

$$\Delta T^* = \beta e^{-\frac{1}{\tau^*} t} \tag{A. 6}$$

$$\frac{d\Delta T^*}{dt} = -\frac{dT_{rm}}{dt}$$

$$= -\frac{1}{\tau}\beta(t)e^{-\frac{1}{\tau^*}} + e^{-\frac{t}{\tau^*}}\frac{d\beta(t)}{dt}. \qquad (A.\ 7)$$

Re-writing Eq. (A. 1) with non-zero $q_{rm}$, and plugging Eqs. (A. 6)-(A. 7) into it, we get

$$\tau\frac{dT_{rm}}{dt} = \Delta T^* + R^*Q_{rm}$$

$$\tau\left(\frac{1}{\tau^*}\beta(t)e^{-\frac{t}{\tau^*}} - e^{-\frac{t}{\tau^*}}\frac{d\beta(t)}{dt}\right) = \beta(t)e^{-\frac{t}{\tau^*}} + R^*Q_{rm}$$

$$R^*Q_{rm} = -\tau^*e^{-\frac{t}{\tau^*}}\frac{d\beta(t)}{dt}. \qquad (A.\ 8)$$

Next, solving for $\beta(t)$ leads to

$$\frac{d\beta(t)}{dt} = -\frac{R^*Q_{rm}}{\tau^*}e^{\frac{t}{\tau^*}}$$

$$\beta(t) = -R^*Q_{rm}\ e^{\frac{t}{\tau^*}} + D, \qquad (A.\ 9)$$

where D is the constant of integration. Plugging Eq. (A. 9) into Eq. (A. 6),

$$\Delta T^* = \left(-R^*Q_{rm}\ e^{\frac{t}{\tau^*}} + D\right)e^{-\frac{t}{\tau^*}}. \qquad (A.\ 10)$$

Let the initial $\Delta T^*$ be $\Delta T^*_{initial} = T^* - T_{initial}$. When $t = 0$,

$$\Delta T^*_{initial} = (-R^*\ Q_{rm}\ e^0 + D)\ e^0$$

$$D = \Delta T^*_{initial} + R^*\ Q_{rm}. \qquad (A.\ 11)$$

Eq. (A. 11) becomes

$$\Delta T^* = \left(-R^*\ Q_{rm}\ e^{\frac{t}{\tau^*}} + \Delta T^*_{initial} + R^*\ Q_{rm}\right)e^{-\frac{t}{\tau^*}}$$

$$= -R^*\ Q_{rm} + \Delta T^*_{initial}\ e^{-\frac{t}{\tau^*}} + R^*\ Q_{rm}\ e^{-\frac{t}{\tau^*}}$$

$$= R^*\ Q_{rm}\left(e^{-\frac{t}{\tau^*}} - 1\right) + \Delta T^*_{initial}\ e^{-\frac{t}{\tau^*}} \qquad (A.\ 12)$$

Then $T_{rm}$ can be written as

$$T_{\text{rm}} = T^* + R^* Q_{\text{rm}} \left(1 - e^{-\frac{t}{\tau^*}}\right) - \Delta T^*_{\text{initial}} \, e^{-\frac{t}{\tau^*}}$$

$$= T_{\text{initial}} \, e^{-\frac{t}{\tau^*}} + (T^* + R^* Q_{\text{rm}}) \left(1 - e^{-\frac{t}{\tau^*}}\right). \tag{A. 13}$$

**Step 3: $T^*$ and $q_{\text{rm}}$ vary but only by a discretized time step.**

As the final step, we assume that $T^*$ and $Q_{\text{rm}}$ vary but remain constant within a time step whose span is $t$. From Eq. (A. 13), the room temperature $T_{\text{rm}}$ at the $(i + 1)^{\text{th}}$ timestep can be written based on the $R^*$, $Q_{\text{rm},i}$ , $\tau^*$, $T_i^*$, and $T_{\text{rm}}$ of the $i^{\text{th}}$ timestep, hence

$$T_{\text{rm},i+1} = T_{\text{rm},i} \, e^{-\frac{t}{\tau^*}} + \left(T_i^* + R^* Q_{\text{rm},i}\right) \left(1 - e^{-\frac{t}{\tau^*}}\right). \tag{A. 14}$$

Throughout the three steps, natural ventilation rate was not considered. Just as $T^*$ and $Q_{\text{rm}}$, treating the airflow rate entering the room from the adjacent zone as a constant that changes only at a discretized time step, $R^*$ and $\tau^*$ become variables, because ventilation rate affects them as in Eqs. (2), (6)-(7) in the main text.

Finally, we get Eq. (A. 15), which was used in Eq. (10) in the main text.

$$T_{\text{rm},i+1} = T_{\text{rm},i} \, e^{-\frac{t}{\tau_i^*}} + \left(T_i^* + R_i^* Q_{\text{rm},i}\right) \left(1 - e^{-\frac{t}{\tau_i^*}}\right) \tag{A. 15}$$

**Bibliography**

[1]   W. O'Brien, I. Gaetani, S. Gilani, S. Carlucci, P.-J. Hoes, and J. Hensen, "International survey on current occupant modelling approaches in building performance simulation," *J. Build. Perform. Simul.*, vol. 10, no. 5–6, pp. 653–671, Nov. 2017, doi: 10.1080/19401493.2016.1243731.

[2]   D. Lai, S. Jia, Y. Qi, and J. Liu, "Window-opening behavior in Chinese residential buildings across different climate zones," *Build. Environ.*, vol. 142, pp. 234–243, Sep. 2018, doi: 10.1016/j.buildenv.2018.06.030.

[3]   S. Pan *et al.*, "A study on influential factors of occupant window-opening behavior in an office building in China," *Build. Environ.*, vol. 133, pp. 41–50, Apr. 2018, doi: 10.1016/j.buildenv.2018.02.008.

[4]   C. Heracleous and A. Michael, "Experimental assessment of the impact of natural ventilation on indoor air quality and thermal comfort conditions of educational buildings in the Eastern Mediterranean region during the heating period," *J. Build. Eng.*, vol. 26, p. 100917, Nov. 2019, doi: 10.1016/j.jobe.2019.100917.

[5]   H. Kim, T. Hong, and J. Kim, "Automatic ventilation control algorithm considering the indoor environmental quality factors and occupant ventilation behavior using a logistic regression model," *Build. Environ.*, vol. 153, pp. 46–59, Apr. 2019, doi: 10.1016/j.buildenv.2019.02.032.

[6]  N. Li, J. Li, R. Fan, and H. Jia, "Probability of occupant operation of windows during transition seasons in office buildings," *Renew. Energy*, vol. 73, pp. 84–91, Jan. 2015, doi: 10.1016/j.renene.2014.05.065.

[7]  V. M. Barthelmes, Y. Heo, V. Fabi, and S. P. Corgnati, "Exploration of the Bayesian Network framework for modelling window control behaviour," *Build. Environ.*, vol. 126, pp. 318–330, Dec. 2017, doi: 10.1016/j.buildenv.2017.10.011.

[8]  H. Mo, H. Sun, J. Liu, and S. Wei, "Developing window behavior models for residential buildings using XGBoost algorithm," *Energy Build.*, vol. 205, p. 109564, Dec. 2019, doi: 10.1016/j.enbuild.2019.109564.

[9]  R. Markovic, E. Grintal, D. Wölki, J. Frisch, and C. van Treeck, "Window opening model using deep learning methods," *Build. Environ.*, vol. 145, pp. 319–329, Nov. 2018, doi: 10.1016/j.buildenv.2018.09.024.

[10] Y. Chen, L. K. Norford, H. W. Samuelson, and A. Malkawi, "Optimal control of HVAC and window systems for natural ventilation through reinforcement learning," *Energy Build.*, vol. 169, pp. 195–205, Jun. 2018, doi: 10.1016/j.enbuild.2018.03.051.

[11] J. von Grabe, "Using the Instance-Based Learning Paradigm to Model Energy-Relevant Occupant Behaviors in Buildings," *Cogn. Comput.*, vol. 12, no. 1, pp. 71–99, Jan. 2020, doi: 10.1007/s12559-019-09672-w.

[12] Z. Wang, L. Yi, and F. Gao, "Night ventilation control strategies in office buildings," *Sol. Energy*, vol. 83, no. 10, pp. 1902–1913, Oct. 2009, doi: 10.1016/j.solener.2009.07.003.

[13] K. Weng, F. Meng, and M. Mourshed, "Model-Based Optimal Control of Window Openings for Thermal Comfort," *Proceedings*, vol. 2, no. 15, Art. no. 15, 2018, doi: 10.3390/proceedings2151134.

[14] J. Landsman, G. Brager, and M. Doctor-Pingel, "Performance, prediction, optimization, and user behavior of night ventilation," *Energy Build.*, vol. 166, pp. 60–72, May 2018, doi: 10.1016/j.enbuild.2018.01.026.

[15] P. Roach, F. Bruno, and M. Belusko, "Modelling the cooling energy of night ventilation and economiser strategies on façade selection of commercial buildings," *Energy Build.*, vol. 66, pp. 562–570, Nov. 2013, doi: 10.1016/j.enbuild.2013.06.034.

[16] Y. Liu *et al.*, "Optimization of top-floor rooms coupling cool roofs, natural ventilation and solar shading for residential buildings in hot-summer and warm-winter zones," *J. Build. Eng.*, vol. 66, p. 105933, May 2023, doi: 10.1016/j.jobe.2023.105933.

[17] ASHRAE, *ASHRAE Guideline 14-2014: Measurement Of Energy, Demand, And Water Savings*. Atlanta, GA: ASHRAE, 2014.

[18] R. Guo, P. Heiselberg, Y. Hu, C. Zhang, and S. Vasilevskis, "Optimization of night ventilation performance in office buildings in a cold climate," *Energy Build.*, vol. 225, p. 110319, Oct. 2020, doi: 10.1016/j.enbuild.2020.110319.

[19] N. Yoon, L. Norford, A. Malkawi, H. Samuelson, and M. A. Piette, "Dynamic metrics of natural ventilation cooling effectiveness for interactive modeling," *Build. Environ.*, vol. 180, p. 106994, Aug. 2020, doi: 10.1016/j.buildenv.2020.106994.

[20] W. Marks, "Multicriteria optimisation of shape of energy-saving buildings," *Build. Environ.*, vol. 32, no. 4, pp. 331–339, Jul. 1997, doi: 10.1016/S0360-1323(96)00065-0.

[21] M. Adamski, "Optimization of the form of a building on an oval base," *Build. Environ.*, vol. 42, no. 4, pp. 1632–1643, Apr. 2007, doi: 10.1016/j.buildenv.2006.02.004.

[22] M. T. Araji and I. Shahid, "A Mathematical Model Toward Energy Optimization with Building-Integrated Photovoltaics," *Technol. Des.*, vol. 1, no. 1, pp. 83–91, May 2017, doi:

10.1080/24751448.2017.1292797.

[23] R. Cheng, X. Wang, and Y. Zhang, "Analytical optimization of the transient thermal performance of building wall by using thermal impedance based on thermal-electric analogy," *Energy Build.*, vol. 80, pp. 598–612, Sep. 2014, doi: 10.1016/j.enbuild.2014.05.023.

[24] A. L. Pisello, V. L. Castaldo, C. Piselli, C. Fabiani, and F. Cotana, "Thermal performance of coupled cool roof and cool façade: Experimental monitoring and analytical optimization procedure," *Energy Build.*, vol. 157, pp. 35–52, Dec. 2017, doi: 10.1016/j.enbuild.2017.04.054.

[25] T. Zakula, P. R. Armstrong, and L. K. Norford, "Modeling Environment for Model Predictive Control of Buildings," *Energy Build.*, vol. 85, pp. 549–559, 2014, doi: 10.1016/j.enbuild.2014.09.039.

[26] G. Carrilho da Graça, N. C. Daish, and P. F. Linden, "A two-zone model for natural cross-ventilation," *Build. Environ.*, vol. 89, pp. 72–85, Jul. 2015, doi: 10.1016/j.buildenv.2015.02.014.

[27] G. Fraisse, C. Viardot, O. Lafabrie, and G. Achard, "Development of a simplified and accurate building model based on electrical analogy," *Energy Build.*, vol. 34, no. 10, pp. 1017–1031, Nov. 2002, doi: 10.1016/S0378-7788(02)00019-1.

[28] S. M. Heibati, F. Atabi, M. Khalajiassadi, and A. Emamzadeh, "Integrated dynamic modeling for energy optimization in the building: Part 1:The development of the model," *J. Build. Phys.*, vol. 37, no. 1, pp. 28–54, Jul. 2013, doi: 10.1177/1744259113475543.

[29] Y. Li and A. Delsante, "Natural ventilation induced by combined wind and thermal forces," *Build. Environ.*, vol. 36, no. 1, pp. 59–71, Jan. 2001, doi: 10.1016/S0360-1323(99)00070-0.

[30] Y. Li *et al.*, "Some examples of solution multiplicity in natural ventilation," *Build. Environ.*, vol. 36, no. 7, pp. 851–858, Aug. 2001, doi: 10.1016/S0360-1323(01)00011-7.

[31] S. D. Fitzgerald and A. W. Woods, "The influence of stacks on flow patterns and stratification associated with natural ventilation," *Build. Environ.*, vol. 43, no. 10, pp. 1719–1733, Oct. 2008, doi: 10.1016/j.buildenv.2007.10.021.

[32] B. Lishman and A. W. Woods, "On transitions in natural ventilation flow driven by changes in the wind," *Build. Environ.*, vol. 44, no. 4, pp. 666–673, 2009, doi: 10.1016/j.buildenv.2008.05.012.

[33] B. Lishman and A. W. Woods, "The effect of gradual changes in wind speed or heat load on natural ventilation in a thermally massive building," *Build. Environ.*, vol. 44, no. 4, pp. 762–772, 2009, doi: 10.1016/j.buildenv.2008.06.026.

[34] O. T. Ogunsola and L. Song, "Application of a simplified thermal network model for real-time thermal load estimation," *Energy Build.*, vol. 96, pp. 309–318, Jun. 2015, doi: 10.1016/j.enbuild.2015.03.044.

[35] G. Capizzi, G. L. Sciuto, G. Cammarata, and M. Cammarata, "Thermal transients simulations of a building by a dynamic model based on thermal-electrical analogy: Evaluation and implementation issue," *Appl. Energy*, vol. 199, pp. 323–334, Aug. 2017, doi: 10.1016/j.apenergy.2017.05.052.

[36] K.-L. He, Q. Chen, E. Dong, W.-C. Ge, J.-H. Hao, and F. Xu, "An improved unit circuit model for transient heat conduction performance analysis and optimization in multi-layer materials," *Appl. Therm. Eng.*, vol. 129, pp. 1551–1562, Jan. 2018, doi: 10.1016/j.applthermaleng.2017.10.149.

[37] Modelica Association, "Modelica Language." Accessed: Sep. 07, 2021. [Online]. Available: https://modelica.org/modelicalanguage.html

[38] J. Neymark and R. Judkoff, "International Energy Agency Building Energy Simulation Test

and Diagnostic Method (IEA BESTEST). Multi-Zone Non-Airflow In-Depth Diagnostic Cases: MZ320 – MZ360," National Renewable Energy Laboratory, Golden, CO, USA, Technical Report NREL/TP-550-43827, 2008. Accessed: Dec. 22, 2017. [Online]. Available: https://www.nrel.gov/docs/fy08osti/43827.pdf

[39] National Renewable Energy Laboratory, "EnergyPlus." Accessed: Mar. 15, 2020. [Online]. Available: https://energyplus.net/

[40] M. Wetter, "Modelica – Spawn of EnergyPlus. 2017 Building Technologies Office Peer Review." U. S. Department of Energy, 2017. Accessed: May 02, 2018. [Online]. Available: https://www.energy.gov/sites/prod/files/2017/04/f34/4_35511_Wetter_031617-1000.pdf

[41] M. Wetter, W. Zuo, T. S. Nouidui, and X. Pang, "Modelica Buildings library," *J. Build. Perform. Simul.*, vol. 7, no. 4, pp. 253–270, Jul. 2014, doi: 10.1080/19401493.2013.765506.

[42] ASHRAE, *ANSI/ASHRAE Standard 140-2017: Standard Method of Test for the Evaluation of Building Energy Analysis Computer Programs*. Atlanta, GA, 2017. Accessed: Jan. 07, 2020. [Online]. Available: https://subscriptions.techstreet.com/products/775077

[43] M. J. Witte, "ANSI/ASHRAE Standard 140 - Input Files - v8.1," EnergyPlus. Accessed: Jan. 27, 2021. [Online]. Available: http://energyplus.helpserve.com/Knowledgebase/Article/View/136

[44] T. Hong and S. H. Lee, "Integrating physics-based models with sensor data: An inverse modeling approach," *Build. Environ.*, vol. 154, pp. 23–31, May 2019, doi: 10.1016/j.buildenv.2019.03.006.

[45] S. Attia *et al.*, "Resilient cooling of buildings to protect against heat waves and power outages: Key concepts and definition," *Energy Build.*, vol. 239, p. 110869, May 2021, doi: 10.1016/j.enbuild.2021.110869.

[46] W. Miller *et al.*, "Conceptualising a resilient cooling system: A socio-technical approach," *City Environ. Interact.*, vol. 11, p. 100065, Aug. 2021, doi: https://doi.org/10.1016/j.cacint.2021.100065.

[47] C. Zhang *et al.*, "Resilient cooling strategies – A critical review and qualitative assessment," *Energy Build.*, vol. 251, p. 111312, Nov. 2021, doi: https://doi.org/10.1016/j.enbuild.2021.111312.

[48] Z. Ai *et al.*, *International Energy Agency - Resilient Cooling of Buildings - State of the Art Review*. Institute of Building Research & Innovation ZT GmbH, 2023. doi: 10.52776/COXK4763.

[49] S. Nateghi and J. Kaczmarczyk, "Multi-objective optimization of window opening and thermostat control for enhanced indoor environment quality and energy efficiency in contrasting climates," *J. Build. Eng.*, vol. 78, p. 107617, Nov. 2023, doi: 10.1016/j.jobe.2023.107617.

[50] Office of Eenergy Efficiency and Renewable Energy, "Spawn-of-EnergyPlus (Spawn)," Energy.gov. Accessed: Jul. 30, 2023. [Online]. Available: https://www.energy.gov/eere/buildings/articles/spawn-energyplus-spawn

[51] T. Nouidui, M. Wetter, and W. Zuo, "Functional mock-up unit for co-simulation import in EnergyPlus," *J. Build. Perform. Simul.*, vol. 7, no. 3, pp. 192–202, May 2014, doi: 10.1080/19401493.2013.808265.

[52] Z. E. Lee and K. M. Zhang, "Scalable identification and control of residential heat pumps: A minimal hardware approach," *Appl. Energy*, vol. 286, p. 116544, Mar. 2021, doi: 10.1016/j.apenergy.2021.116544.

[53] ASHRAE, "Chapter 26: Ventilation and Infiltration," in *ASHRAE handbook—Fundamentals*, [SI ed.]., Atlanta, GA: ASHRAE, 2001.

[54] M. V. Swami and S. Chandra, "Procedures for Calculating Natural Ventilation Airflow Rates in Buildings.," Florida Solar Energy Center, Final Report FSEC-CR-163-86., 1987. [Online]. Available: http://www.fsec.ucf.edu/en/publications/pdf/FSEC-CR-163-86.pdf

[55] W. Zhang, W. Wu, L. Norford, N. Li, and A. Malkawi, "Model predictive control of short-term winter natural ventilation in a smart building using machine learning algorithms," *J. Build. Eng.*, vol. 73, p. 106602, Aug. 2023, doi: 10.1016/j.jobe.2023.106602.